Tellus (1983), *35B*, 142–154

The influence of optical water type on the diurnal response of the upper ocean

By T. D. DICKEY, *Department of Geological Sciences* and *Institute for Marine and Coastal Studies, University of Southern California, Los Angeles, CA 90007 U.S.A.*, and J. J. SIMPSON, *Scripps Institution of Oceanography, La Jolla, CA 92093 U.S.A.*

(Manuscript received January 25; in final form August 4, 1982)

ABSTRACT

The effect of optical water characteristics upon the diurnal variability of upper ocean temperatures and heat content has been studied. A second moment turbulent closure scheme was employed for the simulations. Realistic thermal forcing as well as uniform and time varying wind stresses were used for boundary conditions. The diurnal amplitude in sea surface temperature and long term changes in heat content are strongly influenced by water type for constant wind speeds up to 6 m s^{-1}. The phasing of time-dependent wind stresses can lead to enhanced diurnal sea surface temperature amplitudes (e.g. solar insolation 12 hours out of phase with maximum wind stress). Long term trends in heat content, however, are nearly independent of phase. The results of the simulations are consistent with the range of reported observations. The present work suggests that variability in biological productivity and consequent variations in the optical properties of seawater may be important for realistic modelling of upper ocean structure and climate.

1. Introduction

Diurnal variability in the temperature structure and heat content of the upper ocean has been the focus of several experimental as well as theoretical studies. Few of these efforts, however, have examined the effects of optical water type on either the observed or predicted diurnal structure of the upper ocean. Nonetheless, both numerical models (e.g. Zaneveld *et al.*, 1981; Simpson and Dickey, 1981a, b) and field observations (e.g. Shonting, 1964; Bowden *et al.*, 1970) have appeared in the literature which suggest the need to include proper parameterization of optical absorbance in diurnal studies. Such parameterizations are based on the measured spectral decomposition of the absorption coefficient of natural water (e.g. Jerlov, 1951, 1955; Kullenberg *et al.*, 1970; Tyler and Smith, 1970; Højerslev, 1973, 1974; Morel, 1974; Morel and Prieur, 1975; Ivanoff, 1977; Paulson and Simpson, 1977; Smith and Baker, 1981; Tyler and Smith, 1970; Zaneveld *et al.*, 1979). These observations show significant differences in the optical absorbance characteristics between Type I and Type III water as defined by Jerlov (1976). Because the primary energy source to the ocean is the downward irradiance, one expects that the diurnal structure of the upper ocean is sensitive to the manner in which light is absorbed as a function of both wavelength and depth.

Recent studies have appeared in the literature which partially explored this possibility (e.g. Zaneveld *et al.*, 1981; Simpson and Dickey, 1981a, b). These studies, however, used constant surface thermal and wind stress boundary conditions. The purpose of the present study is to examine the diurnal response of the upper ocean over a wide range of wind speeds and thermal forcing conditions typical of summer and winter diurnal cycles. Downward irradiance parameterizations characteristic of both open-ocean (Type I) and coastal (Type III) water are used to determine differences in the diurnal response of these dissimilar oceanic regimes. In addition, the sensitivity of diurnal upper ocean structure to the phase relationship between the wind stress and surface heating is investigated.

2. Observations

Observations taken in several different locations indicate that the diurnal response occurs in all

Table 1. *Summary of more recent observations of diurnal variability in the upper ocean. These observations are representative of several regions of the world's ocean*

Author	Month	ΔT (°C)	Winds (m s^{-1})	Latitude
Bowden *et al.* (1970)	July	0.23	7–8	34°55′ N
Delnore (1972)	June	0.13–0.40	5–8	15°00′ N
Halpern and Reed (1976)	March	0.9–1.4	2	21°40′ N
Hoeber (1972)	February	0.15	6–8	7°18′ N
Howe and Tait (1969)	July	0.2	7	34°55′ N
Kondo *et al.* (1979)	March, April, September	1.0	<5	
		0.1–0.3	5–7	35°08′ N
		<0.1	<10	
Ostapoff and Worthem (1974)	September–October	0.96–1.70	6–7	21°00′ N
Shonting (1964)	May	1.0	2–7	24°40′ N
Simpson and Paulson (1979a)	January, February	0.1–0.2	5	35°00′ N

seasons with the reported range of diurnal sea surface temperatures (ΔT) lying between <0.1 °C and 1.7 °C (Table 1). Observations were chosen for citation in Table 1 because they were usually made with a salinity, temperature, depth (STD) or conductivity, temperature, depth (CTD) measuring instrument. In general, the maximum net heating at the surface leads the maximum sea surface temperature by two to four hours (e.g. Stommel and Woodcock, 1951; Shonting, 1964; Halpern and Reed, 1976). The observed depth of maximum penetration of the discernible heat wave typically lies within the range of 5 m to 30 m (e.g. Leetmaa and Welch, 1972; Howe and Tait, 1969). Maximum isothermal penetration lags maximum surface heating. The corresponding thermal response is such that heating occurs at a greater rate than cooling, which results in an asymmetric diurnal temperature wave (Shonting, 1964).

The experimental data have led to a general understanding of diurnal variability. The interpretation of the individual data sets, however, is complex. Effects which lead to this difficulty include: advection, internal gravity waves, tides, and ship drift along with variations in cloud cover and water turbidity. For these reasons, direct diurnal simulations are precluded until a more complete and less ambiguous data set is available.

3. Surface boundary conditions

The total heat flux at the air–sea interface can be written

$$Q_T = (1 - \alpha)Q_S + Q_{BC} - Q_B - Q_L - Q_{SE} \qquad (1)$$

where Q_T is the total heat flux into the ocean, Q_S is the incident solar flux, α is the albedo of the sea surface, Q_{BC} is the downward long-wave flux emitted from the atmosphere, Q_B is the upward long-wave flux emitted from the sea surface, Q_L is the latent heat flux, and Q_{SE} is the sensible heat flux. Heat gained by the ocean is considered positive. The second term in (1) represents the short-wave flux which penetrates the sea surface and dominates the heat budget of the upper ocean. The net long-wave flux, $-Q_{BN}$, may be introduced in (1) to replace $Q_{BC} - Q_B$. Frequently, it is as large as the latent heat flux. Generally, the sensible heat flux is small compared to the latent heat flux over the ocean.

The summer diurnal thermal boundary conditions used in this study were constructed from (1). They are typical of the central Pacific (35° N). In August, however, the incident solar flux over the entire latitude range between 10° N and 45° N is within ±7% of the value at 35° N (List, 1951). Hence, the results discussed in this paper have general applicability to a large geographical region of the ocean. Methods used to estimate the individual terms in (1) for clear skies are discussed below.

3.1. *Short-wave flux*

The hourly short-wave flux reaching the sea surface was calculated with the statistical relation of Lumb (1964)

$$Q_S = 135fs \qquad (2)$$

where $f = a + bs$ is the fraction of solar flux transmitted through the atmosphere, s is the mean of the sines of the solar altitude at the beginning

and end of the hour, and a and b are constants from one of nine categories of atmospheric conditions representative of the hour period. The coefficient in (2) is the solar constant. Mean hourly values of solar altitude were calculated from the latitude, solar declination and hour angle. For nearly clear skies ($c < 2$ oktas), $a = 0.61$ and $b = 0.20$. Eq. (2) gives values of Q_S in mW cm^{-2}. These values were converted to W m^{-2} because all the calculations in this paper are done in the MKS system. Simpson and Paulson (1979b) have shown that daily predictions of Q_S from (2) can be made with an accuracy of $\pm$ 10 W m^{-2}.

The albedo of the sea surface is a function of the solar altitude, θ, and the atmospheric transmittance, Γ (Payne, 1972; Simpson and Paulson, 1979b). For the clear sky case ($\Gamma \rightarrow 1.0$) the albedo is dependent only on solar altitude. Hourly values of albedo were obtained from tables given by Payne (1972) and by Simpson and Paulson (1979b). Diurnal variations in the albedo of the sea surface contribute little to the thermal boundary condition because the albedo is large only for low solar altitudes when the incident solar flux, Q_S, is near zero. Near midday, the albedo approaches an asymptotic value of 0.04 for summer and 0.06 for winter. Time series of the short-wave heating functions used in this study (summer) are shown in Fig. 1.

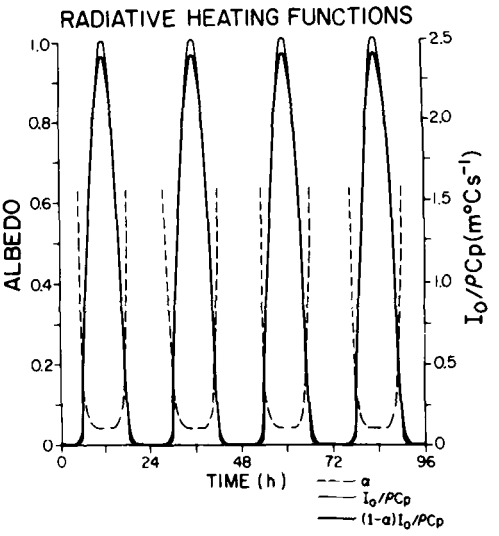

Fig. 1. Time series of the incident solar flux ($I_0/\rho c_p$), the albedo of the sea surface (α), and the net solar flux ($1 - \alpha$) $I_0/\rho c_p$, typical of summer. All fluxes are normalized.

3.2. *Long-wave flux*

The net long-wave flux was assumed constant over a diurnal cycle. This assumption is reasonable under clear sky conditions because variability in the net long-wave flux is influenced primarily by changes in cloud type, amount and height (Simpson and Paulson, 1979b). The value of $Q_{BN} = 62$ W m^{-2} was based on direct flux measurements of the net long-wave flux over the open ocean in winter under clear skies (Simpson and Paulson, 1979b). The same value was used for the summer simulations since the net long-wave flux varies only slightly with season (Wyrtki, 1966). This occurs because the ratio of the seasonal change in sea surface temperature (ΔT) to the annual mean (T) is small (i.e. $\Delta Q_{BN}/Q_{BN} \propto 4\,\Delta T/T$), where T is in degrees Kelvin. Evaluation of $\Delta Q_{BN}/Q_{BN}$ for typical mid-latitude seasonal changes in ΔT shows that the seasonal variation is only about 10%. In addition, Q_{BN} varies even less regionally (Wyrtki, 1966).

3.3. *Turbulent heat fluxes*

Hourly values of the sensible and latent heat flux were computed with the bulk formulas (e.g. Malkus, 1962; Friehe and Schmitt, 1976)

$$Q_{SE} = \rho_a c_{p_a} C_{10} U_{10} (T_s - T_a) \tag{3}$$

$$Q_L = \rho_a L C_{10} U_{10} (q_s - q_a) \tag{4}$$

where ρ_a is the density of air, c_{p_a} is the specific heat of air, C_{10} is the drag coefficient, L is the latent heat of evaporation, U_{10} is the mean wind speed at 10 m, T_s is the sea surface temperature, T_a is the air temperature at 10 m, q_s is the saturation water vapor density at the temperature of the sea surface, and q_a is the water vapor density of air at 10 m. Values of the constants used in eqs. (3) and (4) are given in Table 2. Mean values of the air-sea temperature difference for the month of August, based on the analysis of 20 years of meteorological data from Ocean Weather Station V (35° N) is −0.4 °C (Husby and Seckel, 1975). A corresponding value for the vapor pressure difference is 6.0 mb. These mean differences were used to compute the mean turbulent fluxes of heat. The above mean values of ($T_s - T_a$) and ($q_s - q_a$) were used for all winds speeds because Pedersen and Bøyum (1980) have shown that these quantities are nearly independent of wind speed.

Table 2. *Conditions common to all runs*

Parameter	Symbol	Value
Geostrophic velocity	Ug, Vg	0
Initial mean velocity	U, V	0
Coriolis parameter	f	1.0×10^{-4} s^{-1}
Salinity	S	35‰
Drag coefficient	C_{10}	1.4×10^{-3}
Specific heat of water	c_p	4.0×10^3 kg^{-1} °C^{-1}
Specific heat of air	c_{pa}	9.96×10^2 kg^{-1} °C^{-1}
Density of air	ρ_a	1.26 kg m^{-3}
Net long-wave flux	Q_{BN}	62 W m^{-2}
Latent heat of evaporation	L	2.26×10^6 kg^{-1}

3.4. *Wind stress*

The wind stress was calculated from the empirical equation (e.g. Friehe and Schmitt, 1976)

$$\tau_{ox} = \rho_a C_{10} U_{10}^2 \tag{5}$$

Simulations were run with both uniform and time dependent wind speeds.

4. Downward irradiance

The parameterization of the absorbance of downward irradiance, based on observations by Paulson and Simpson (1977), is given by

$$I(z) = I_0\{R \exp(z/\zeta_1) + (1 - R)\exp(z/\zeta_2)\} \tag{6}$$

where $I(z)$, the downward irradiance, is the radiant flux density on a horizontal surface due to contributions from the entire upward hemisphere, and I_0 is the incident less reflected and emergent irradiance at the sea surface. The two attenuation lengths ζ_1 and ζ_2 and the irradiance constant R were determined empirically for various water types. This general form was originally suggested by Emden (1913). Preferential absorption of the red spectral components in the upper few meters is characterized by the first term in (6) while the absorption of blue-green light below a depth of about 10 m is characterized by the second term (i.e., $\zeta_2 > \zeta_1$). Absorption of the ultraviolet in the near surface layer was not explicitly included in (6) because the heat contribution in the ultraviolet region is relatively small compared to that in the red region of the spectrum. Values of the irradiance constants, ζ_1, ζ_2, and R, used in this study are given in Table 3.

Table 3. *Empirical forms used to test the sensitivity of the upper ocean structure to the water type* (eq. 6)

Water type	R	ζ_1 (m)	ζ_2 (m)
Type I	0.580	0.35	23
Type III	0.780	1.4	7.9

Simpson and Dickey (1981a) have shown that for relatively low wind speeds ($U_{10} \leqslant 10$ m s^{-1}) significantly different dynamics and structure occur within the mixed layer when (6) is used instead of the commonly used single exponential parameterization of downward irradiance. Parameterizations of downward irradiance more complicated than eq. (6) (e.g. Zaneveld and Spinrad, 1980; Simpson and Dickey, 1981b) could have been used for this study. However, Simpson and Dickey (1981b) used both a spectral decomposition of the incident solar radiation and an arctangent model of downward irradiance and found that such parameterizations of downward irradiance result in dynamics and structure essentially identical to those obtained with (6). These same studies also show that the traditional single exponential appears to be acceptable *only* at very high winds ($U_{10} > 20$ m s^{-1}). Diurnal variability is usually associated with relatively low wind speeds (see Table 1). Hence, only the double exponential parameterization of the absorbance of downward irradiance (i.e., eq. 6) is used in this paper.

The depth-integrated irradiance flux divergence may be defined as

$$F(z) = \int_z^0 \frac{\partial I(z)}{\partial z}\,dz = \int_z^0 dI(z) = I(0) - I(z)$$

This quantity is normalized by the incident less reflected irradiance at the surface, I_0. Vertical profiles of $F(z)/I_0$ for both Type I and Type III water are shown in Fig. 2. A cross-over occurs between these profiles. A similar cross-over occurs at approximately the same depth in data and in irradiance parameterizations discussed by Ivanoff (1977). The arctangent parameterization of downward irradiance (Zaneveld and Spinrad, 1980) also was used to compute $F(z)$. Again, a cross-over occurred but at a somewhat shallower depth. Such cross-overs are not inconsistent with the integral constraint that for a given value of I_0, $F(z)$ must

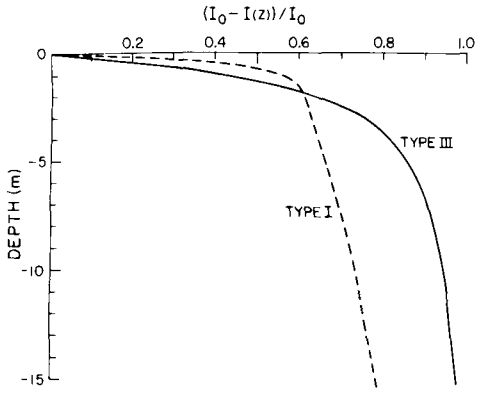

Fig. 2. Vertical profiles of the depth-integrated component of absorbed downward irradiance for both Type I and Type III water.

converge to the value I_0 regardless of the functional form of $I(z)$. A physical interpretation of this integral constraint is that the photon flux (e.g., energy) is conserved. Such cross-overs are not surprising because observed profiles of downward irradiance measure the *in situ* distribution of light which in Type III coastal waters result not only from absorption but also from scattering (Pak *et al.*, 1970; Kullenberg, 1974; and Zaneveld, private communication), nepheloid layers (Stavn, 1982), and marine snow (Trent *et al.*, 1978). Reported parameterizations of downward irradiance, however, generally assume a homogeneous optical medium. Further, they do not model most of the optical processes which are known to affect Type III water. The physical processes discussed above, with the singular exception of absorption, can differentially redistribute light as a function of depth and wavelength prior to absorption. The resulting Type III irradiance profile, therefore, may depart substantially from that of a simple absorption model. The degree of departure from the simple absorption model of Type III water necessarily is time-dependent because biological productivity and river outflow, the sources of the optical scatters in Type III water, are non-steady processes. At present, oceanic measurements do not exist with which to sort out the individual contributions to $I(z)$ for Type III water. Our approach is to model Type III water with a *mean* irradiance profile which is internally consistent with other reported optical measurements. This approach is adequate for most dynamical purposes.

5. Model

Field observations (e.g. Kullenberg, 1971) show that stratification and vertical shear are two of the primary factors which determine the degree of vertical diffusion in the water column. Kullenberg's experimental results establish some of the general criteria for the selection of a numerical model capable of reliably predicting upper ocean structure. Specifically, such a model must be able to determine the vertical profiles of mean fluid properties as functions of a Richardson number. The level $2\frac{1}{2}$ version of the Mellor-Yamada (1974) turbulent closure scheme (e.g. Yamada, 1977; Blumberg and Mellor, 1981; Simpson and Dickey, 1981a) was chosen for the present study in part because it satisfies the above criteria and also because it has the capacity to distribute downward irradiance differentially with depth rather than in an integrated fashion as would be required by an integral model. A detailed description of the model is given by Blumberg and Mellor (1981). The conservation of heat equation presented here differs from that used by Mellor and Durbin (1975) and by Blumberg and Mellor (1981) because the divergence of the downward irradiance is included. This change was introduced by Simpson and Dickey (1981a). The modified equation is

$$\rho c_p \frac{\partial T}{\partial t} + \rho c_p \frac{\partial}{\partial z} \overline{w'T'} = \frac{\partial I}{\partial z} \tag{7}$$

where T is the mean temperature, ρ is the *in situ* density (Fofonoff, 1962) and c_p is the specific heat of sea water. The first term in (7) is the local rate of change of heat, the second term is the vertical divergence of the turbulent heat flux, and the right-hand side of (7) is the vertical divergence of the downward irradiance flux. Vertical integration of (7) yields

$$\frac{\partial H}{\partial t} + \rho c_p |\overline{w'T'}(0) - \overline{w'T'}(z)| = F(z)$$

where H is the heat content per unit area and $F(z)$ is defined as in section 4.

The level $2\frac{1}{2}$ version includes the diffusion of turbulent kinetic energy in the local turbulent energy balance. Simpson and Dickey (1981a, b) have shown that this term is important at low wind speeds because the primary balance between shear-production and dissipation, as observed in

the mixed layer under high wind speeds, is no longer valid. The vertical grid spacing was optimized with a logarithmic distribution so that the number of computational grid points is greatest near the surface. There are 101 levels for the upper 50 m. This is ideal for including the vertical divergence of downward irradiance. The time step was one hour. Model sensitivity to both time-step and grid spacing was discussed by Simpson and Dickey (1981a, b). Their results show that the spatial and temporal resolution cited above is adequate to model the diurnal response of the upper ocean. Simulations were run for 96 hours and minimal effects of spin-up were observed during the first few hours. Conditions common to all runs are given in Table 2.

6. Results

6.1. *Summer, constant* τ

Sea surface temperature as a function of time for uniform wind speeds of 0, 2, 4, 6 and 9 m s^{-1} is shown in Fig. 3. This range of wind speeds was selected on the basis of the observations which are summarized in Table 1. For wind speeds less than 3 m s^{-1} the diurnal amplitude in sea surface temperature is larger for Type I water than for Type III water. The reverse is true for wind speeds greater than 3 m s^{-1}. For wind speeds 6–9 m s^{-1}, however, the diurnal amplitude in sea surface temperature is less dependent upon water type. At a wind speed of 9 m s^{-1}, the sea surface temperature decreases as a function of time because the wind is sufficiently strong to produce a sustained deepening of the well-mixed layer. Isotherms as functions of time and depth for $U_{10} = 2$ and 6 m s^{-1} are shown in Figs. 4–5, respectively. For a wind speed of $U_{10} = 2$ m s^{-1}, the diurnal response primarily is confined to the upper 5 m, whereas for $U_{10} = 6$ m s^{-1} the depth of penetration is approximately 15 m. At $U_{10} = 2$ m s^{-1}, Type I ($\zeta_1 = 0.35$ m) shows a more intensified thermal gradient at the base of the mixed layer compared to that associated with Type III ($\zeta_1 = 1.4$ m). At $U_{10} = 6$ m s^{-1}, however, the relative intensities of these thermal gradients are reversed. This behavior as well as the transition noted in sea surface temperature amplitudes results from the fact that at low wind speeds the thermal structure is primarily influenced by the length scale ζ_1, whereas for higher

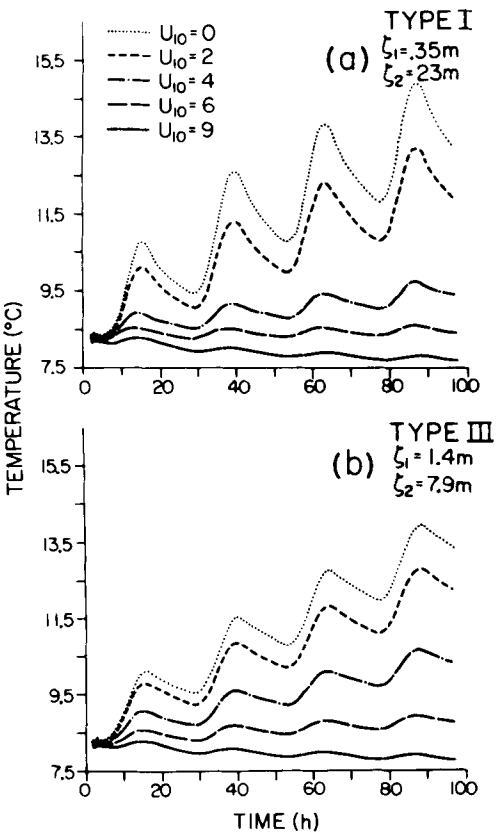

Fig. 3. Times series of sea surface temperature for wind speeds of 0, 2, 4, 6, and 9 m s^{-1} for (a) Type I ($\zeta_1 = 0.35$ m), and (b) Type III ($\zeta_1 = 1.4$ m). (Constant τ, summer.)

wind speeds the ζ_2 length scale has increasing importance (see Fig. 2). This effect is discussed in detail by Simpson and Dickey (1981a).

A noticeable asymmetry exists in the isotherms of Figs. 4–5. This asymmetry results in part from the fact that the net rate of heating of the water column during the day greatly exceeds the net rate of cooling during the night. Thus, enhanced stability created during the day impedes mechanical mixing at night. Shonting (1964) suggested that the Richardson number increased rapidly during the day and could account for a similar asymmetry found in his observations. Contours of flux Richardson number (the ratio of negative buoyancy production to shear production) corresponding to the isotherms in Fig. 5 are shown in Fig. 6. Three distinct regimes of flux Richardson

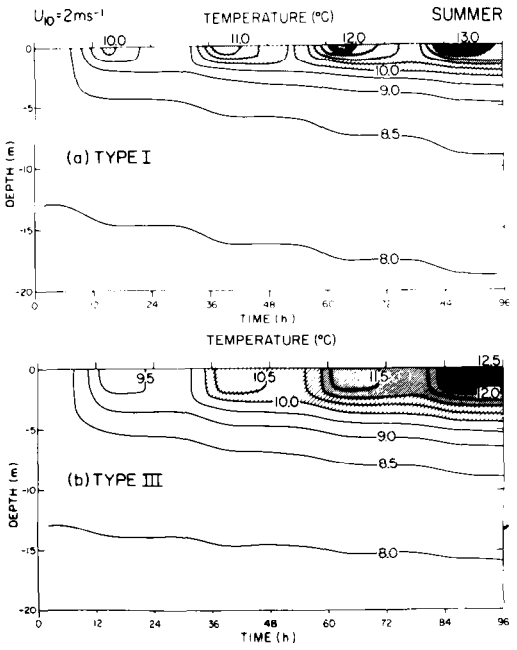

Fig. 4. Isotherms as functions of depth and time for U_{10} = 2 m s^{-1} for (a) Type I, and (b) Type III. (Constant τ, summer).

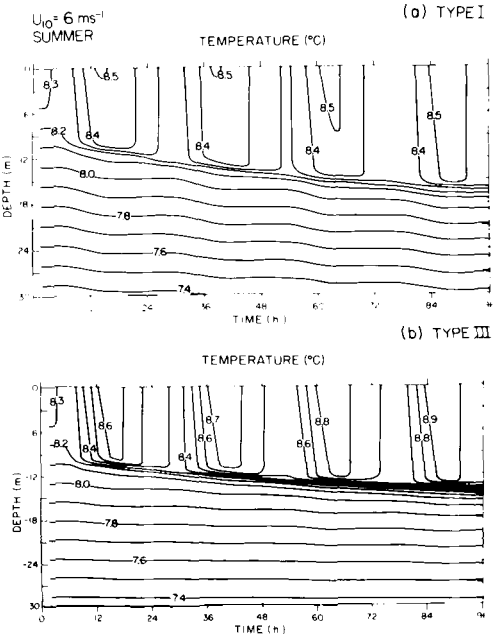

Fig. 5. Isotherms as functions of depth and time for U_{10} = 6 m s^{-1} for (a) Type I, and (b) Type III. (Constant τ, summer.)

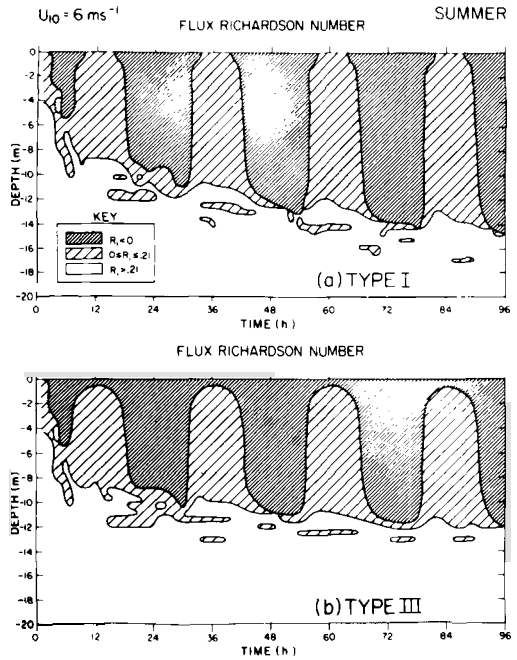

Fig. 6. Flux Richardson numbers as functions of depth and time for U_{10} = 6 m s^{-1} for (a) Type I, and (b) Type III. (Constant τ, summer.)

number are defined: (1) stable, $R_i > 0.21$; (2) turbulent and convectively stable, $0 \leqslant R_i \leqslant 0.21$; and (3) turbulent and convectively unstable, $R_i < 0$. These contours show that the mixed layer continues to deepen slightly throughout the U_{10} = 6 m s^{-1} simulation. At night, the flow regime throughout most of the mixed layer is turbulent and convectively unstable. Often, at the base of the mixed layer there is a small region of turbulent but convectively stable water. During the day, the water column is turbulent and convectively stable for Type I water. For Type III water, however, a shallow layer of convectively unstable water persists at the surface. This difference in stability between Type I and Type III water is attributable to differences in the length scales ζ_1 and ζ_2 associated with these two water types. Intermittent patches of convectively stable though turbulent water are embedded in the more stable thermocline. These manifest themselves as multiple mixed layers frequently reported in the literature (e.g. Thorpe, 1977; Simpson and Paulson, 1979a; Defant, 1981), and result from localized shear instability. These general features show that the local structure of turbulence evolves in time. Three

mechanisms of turbulence generation are active. They are: positive buoyancy production, surface-generated shear production, and localized interior shear production. The relative importance of these production terms, however, varies in both space and time.

Time series of temperature for various depths were compared for a simulation using a wind speed of 2 m s^{-1}. The peak sea surface temperature lags the peak incident solar flux by approximately 3.5 hours. This lag is consistent with observations reported by Shonting (1964) and by Ostapoff and Worthem (1974). The depth dependence of the phase lag between peak sea surface temperature and the thermal wave at depth agrees well with observations reported by Howe and Tait (1969), Bowden *et al.* (1970), and by Halpern and Reed (1976). Slight inversions develop after sunset. Such inversions have been reported in the literature (e.g. Thorpe, 1977; Defant, 1981). These inversions are consistent with the flux Richardson numbers discussed previously. A detailed explanation for the occurrence of these inversions is given by Simpson and Dickey (1981a). Analogous time series for U_{10} = 6 m s^{-1} show that the amplitudes and phase lags of these thermal waves are diminished compared to those of the U_{10} = 2 m s^{-1} simulations. In addition, the depth of penetration of the thermal wave is much deeper, approximately 12 m. A significant difference occurs between the Type I (ζ_2 = 23 m) and Type III (ζ_2 = 7.9 m) simulations for U_{10} = 6 m s^{-1}. Both the amplitudes and the rate of increase of the mean temperatures are greater for Type III water than for Type I water. This result is consistent with the different optical properties of the two water types.

The heat content per unit area of a water column of depth h is given by

$$H = c_p \int_{-z}^{0} \rho(z) T(z)\, dz \qquad (9)$$

where $\rho(z)$ is the *in situ* density, c_p is the heat capacity of saltwater at constant pressure, here assumed independent of depth, and $T(z)$ is the vertical profile of temperature. The integration was limited to a depth of h = 35 m. This depth was well below any actively turbulent region of the water column for all the reported simulations. Time series of H for Type I and Type III water under wind speeds of 2 and 6 m s^{-1} are shown in Fig. 7. The diurnal amplitude in the heat content is nearly

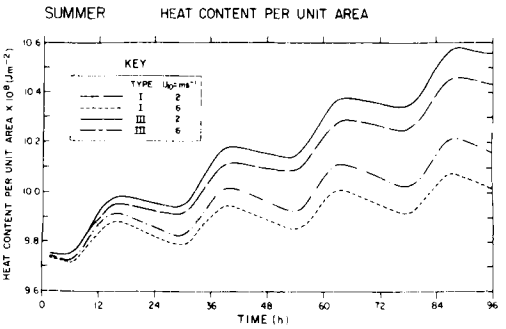

Fig. 7. Time series of heat content per unit area for Type I and Type III water under wind speeds of 2 and 6 m s^{-1}.

independent of water type and wind speed. The mean rate of increase of the heat content, however, is dependent on both water type and wind speed. Maximum mean rate of increase in the heat content occurs for the Type III simulation with U_{10} = 2 m s^{-1}. The minimum occurs for Type I simulations with U_{10} = 6 m s^{-1}. Type I at U_{10} = 2 m s^{-1} and Type III at U_{10} = 6 m s^{-1} lie between these two extremes in consecutive order. This arrangement of curves is consistent with the generally higher heat absorption characteristic of Type III water compared to Type I and the larger entrainment rates at the base of the mixed layer associated with U_{10} = 6 m s^{-1} compared to U_{10} = 2 m s^{-1}.

6.2. *Summer, variable τ*

There has been, to our knowledge, no study of the sensitivity of upper ocean structure to a phase-dependent wind stress with respect to diurnal thermal forcing. Kondo *et al.* (1979), however, implied that such wind variability would affect the response of the mixed layer. The effect of such a set of boundary conditions on diurnal thermal structure is examined here. The general periodic function is given by

$$\begin{aligned}
&t \leqslant 4 && U_{10} = 0\\
&4 + nP < t \leqslant 6 + nP && U_{10} = \frac{U_{\max}}{2} |t - (4 + nP)|\\
&6 + nP < t \leqslant 18 + nP && U_{10} = U_{\max}\\
&18 + nP < t \leqslant 20 + nP && U_{10} = U_{\max} \times \left\{1 - \frac{|t - (18 + nP)|}{2}\right\}\\
&20 + nP < t \leqslant 28 + nP && U_{10} = 0
\end{aligned} \qquad (10)$$

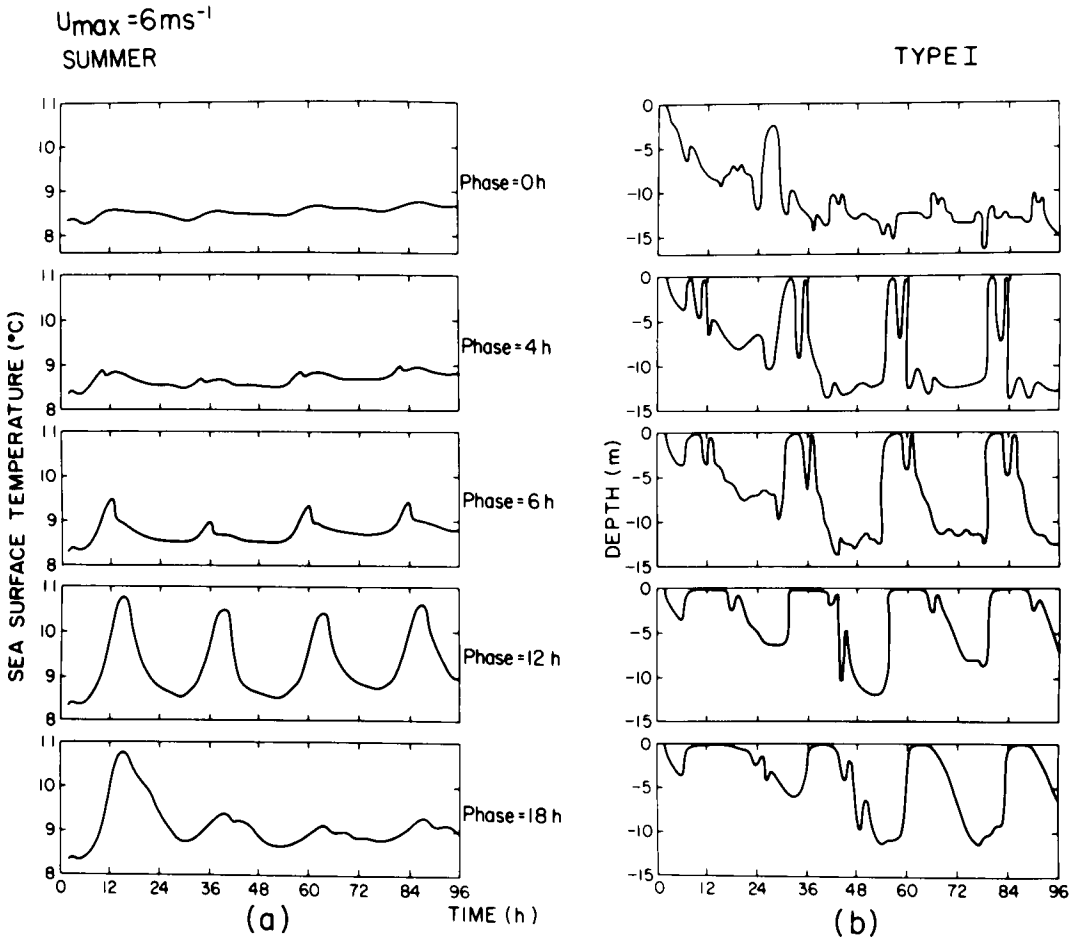

Fig. 8. (a) The sea surface temperature time series. (b) The mixed layer depth time series with wind phases. Both use wind phases of 0, 4, 6, 12 and 18 h. (Summer, variable τ.)

where t is time in hours, P is period and equal to 24 hours, and $n = 0, 1, 2, 3$. The amplitude U_{10} is $U_{max} = 6$ m s^{-1}. The form of this wind forcing was chosen to include a gradual onset and cessation of the wind field in order to minimize inertial effects. The reference for the time base is the insolation wave. Thus, a phase shift of 4 hours means that the onset of the transition from 0 to 6 m s^{-1} occurs 4 hours later. The phases chosen are 0, 4, 6, 12 and 18 hours. For the phase-dependent simulations, only results for Type I water are presented.

Time series of sea surface temperature and mixed layer depth for phase lags of 0, 4, 6, 12 and 18 hours are shown in Fig. 8. The transient state is confined to the first 30 hours. Minimum amplitude in the sea surface temperature occurs when the phase lag between insolation and wind is 0 hours. The maximum amplitude occurs for a phase lag of 12 hours. These results are consistent with the fact that under these conditions maximum insolation coincides with maximum wind stress. Thus, sufficient mechanical energy is available to prevent the build-up of a strong stratification near the surface. At night, however, no mechanical energy is available for mixing, and the only source of positive buoyancy production is net long-wave radiative cooling at the surface. This production of turbulent kinetic energy is insufficient to overcome the thermal gradients established during the day. This budget of turbulent kinetic energy is reflected in the time series of the mixed layer depth shown in Fig. 8. For a phase lag of 12 hours, however, strati-

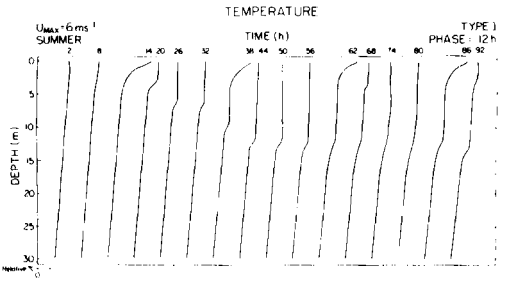

Fig. 9. Sequence of temperature profiles for phase = 12 h. (Summer, variable τ.)

fication increases at a greater rate during the day because there is no mechanical energy available for turbulent mixing. This effect may be seen in Fig. 9 by comparing temperature profiles at 8 and 14 hours. The resulting daytime mixed layer is quite shallow. Thus, by the conservation of heat, the daytime sea surface temperatures are significantly greater. At night, both mechanical mixing and positive buoyancy production are maximum and thus the turbulent kinetic energy is sufficient to rapidly erode the previously established stratification. Phase lags of 0 and 12 hours represent the extreme responses of the diurnal mixed layer.

The high degree of variability in mixed layer depth (Fig. 8b) may be best understood by considering the sequence of temperature profiles seen in Fig. 9. The formation of multiple mixed layers is shown in the series of profiles for 56 through 80 hours. At 56 hours, active mixing has produced an approximately isothermal layer to a depth of about 13 m. With the onset of radiative heating, a very shallow mixed layer, bounded by an intense thermocline, develops at 62 hours. Subsequent mixing begins to erode this shallow thermocline and produces a mixed layer with a depth of about 4 m which is superimposed upon the deeper mixed layer formed at 56 hours. Continued deepening may be seen until 80 hours, when the mixed layer depth is about 13 m. Intermediate phases indicate even more pronounced multiple mixed layer structure. Previous energy arguments explain this detailed structure. Multiple mixed layers also may form under constant wind speed conditions (see Fig. 6).

Contours of temperature as functions of depth and time are shown for phase lags of 0 and 12 hours in Figs. 10a and b, respectively. Corresponding contours of the flux Richardson number are shown in Figs. 11a and b. The intensity of the thermocline is much greater for the phase lag of 12 hours. Below the 8° isotherm, however, the structure associated with the two simulations is quite similar. For a phase lag of 0 hours, the near surface flux Richardson number alternates between regions which are convectively unstable and those which are convectively stable, though turbulent. Generally, for a phase lag of 12 hours, the near surface flux Richardson number alternates between regions which are convectively unstable and those which are stable. The periods of time during which the water column is convectively unstable are nearly independent of phase lag. For a phase lag of 0 hours during the day, mechanical mixing occurs at the surface. For a phase lag of 12 hours, however, the daytime near surface layer is not subject to mechanical mixing. For zero lag (Fig. 11a) the turbulent energy balance is dominated by near-surface shear production (daytime) and positive buoyancy production (night-time). Localized regions of internal shear appear to correlate well with the occurrence of multiple mixed layers in the water column. For the 12-hour lag (Fig. 11b), however, the turbulent energy balance is dominated by positive buoyancy production (night) and to a much lesser degree surface-generated shear production. The vertical profiles of temperature in Fig. 9 show numerous regions of high variability in static stability separated by regions of nearly neutral stability. Such regions serve as localized centers of intense interior shear production.

Time series of the heat content per unit area for phase shifts of 0, 4, 6, 12 and 18 hours were computed. The diurnal amplitude in these time series is a weak function of phase. Maximum amplitude occurs for a phase shift of 12 hours while minimum amplitude occurs for a phase shift of 0 hours. The mean rate of change of heat content per unit area per unit time, however, is nearly independent of phase. Under uniform wind stress, the mean trends in the rate of change of heat content per unit area per unit time diverge as functions of both wind speed and water type (see Fig. 7). It may be concluded that water type and wind speed are at least as important as wind phasing for determining long-term variations in upper ocean heat content. The present results support the conjecture that cycles in biological productivity, and hence annual variations in the optical properties of seawater,

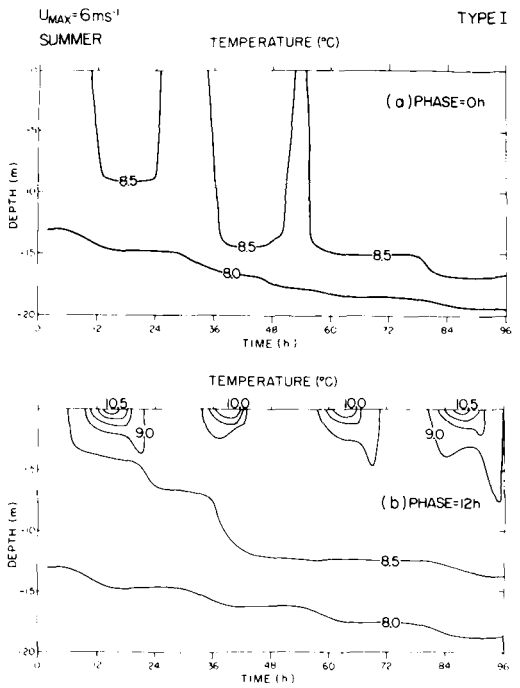

Fig. 10. Isotherms as functions of depth and time for (a) phase = 0 h, and (b) phase = 12 h. (Summer, variable τ.)

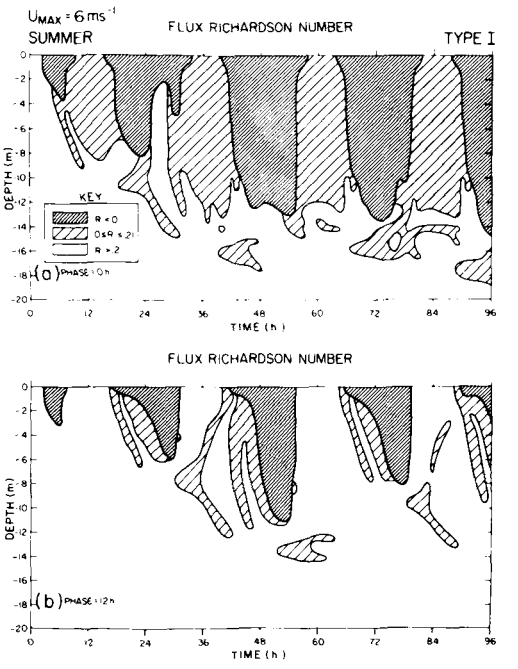

Fig. 11. Flux Richardson numbers as functions of depth and time for (a) phase = 0 h, and (b) phase = 12 h. (Summer, variable τ.)

may need to be included in realistic global climate models.

6.3. *Additional considerations*

All of the runs previously discussed used a constant value of the drag coefficient equal to 1.4×10^{-3}. The same value was used for both momentum and heat. This was done to facilitate the intercomparison between individual results. Recent observations by Large and Pond (1981), however, have shown that for neutrally stable conditions $C_{10} = 1.2 \times 10^{-3}$ for wind speeds between 4 and 11 m s^{-1}. Anderson and Smith (1981) indicate that the exchange coefficient for water vapor under neutral conditions is 1.3×10^{-3}. It is reasonable to use a similar value for turbulent heat exchange since scalars are expected to transfer similarly. Our value of 1.4×10^{-3} is consistent with the majority of observations reported in the literature. Nonetheless, we made an intercomparison between runs with $C_{10} = 1.2 \times 10^{-3}$ and with $C_{10} = 1.4 \times 10^{-3}$ for Type III water. Use of a lower drag coefficient slightly enhances the diurnal variability and increases the mean rate of heating of the water column as expected because both free convection and mechanical mixing are diminished. The effect of atmospheric stability generally will not change the value of the drag coefficient for conditions simulated here by more than + 10% of the neutral value (Deardorff, 1968).

In the uniform wind speed cases previously described, the wind was initially applied as an impulse. Inertial oscillations were consequently present. For comparison, inertial effects were suppressed by initially applying the wind as a ramp function for a duration of one inertial period. The results were virtually unchanged.

7. Concluding remarks

Runs also were performed for typical winter forcing (February). The following general conclusions can be drawn. The magnitude of the diurnal signal in sea surface temperature is typically less in winter than in summer. Moreover, the magnitude of the diurnal response is signi-

ficantly more latitude dependent than the summer diurnal response because the latitudinal variation in solar flux is much greater in winter than in summer (see List, 1954). There may be an appreciable wintertime diurnal signal in sea surface temperature under particular forcing conditions (i.e., 12-hour phase shift between heating and wind stress). Also, the wintertime diurnal variation in mixed layer depth is greater than that of summer. Wintertime structure results from the same three turbulence mechanisms; only the rates of production and their relative spatial and temporal evolution differ. Such differences in intensity are due primarily to seasonal differences in the thermal boundary condition.

In summary, the simulated diurnal structure discussed in this study is consistent with the range of observations reported in the literature. Further, the results imply that inclusion of cycles in biological productivity, and hence variations in the optical properties of seawater, may be required for realistic global climate models.

8. Acknowledgements

The authors would like to express their thanks to Professor J. L. Reid and Dr. Kern Kenyon for their most helpful suggestions and comments. We would also like to thank Dick Schwartzlose and the MLRG business office for helping to find the money. The manuscript was typed by Sharon McBride and editorial assistance was provided by Kittie Kuhns. Fred Crowe and the MLRG Illustrations Group prepared the figures. Support for this work was provided by the Office of Naval Research (Optical Dynamics Experiment, contract #2-3207-02), the Department of Geological Sciences and the Institute for Marine and Coastal Studies, University of Southern California, and the Marine Life Research Group of the Scripps Institution of Oceanography.

REFERENCES

Anderson, R. J. and Smith, S. D. 1981. Evaporation coefficient for the sea surface from eddy flux measurements. *J. Geophys. Res. 86*, 449–456.

Blumberg, A. F. and Mellor, G. L. 1981. A coastal ocean numerical model. In *Mathematical modelling of estuarine physics* (ed. J. Sundermann and K.-P. Holz). Berlin/New York: Springer-Verlag, 203–219.

Bowden, K. F., Howe, M. R. and Tait, R. I. 1970. A study of the heat budget over a seven-day period at an oceanic station. *Deep-Sea Res. 17*, 401–411.

Deardorff, J. W. 1968. Dependence of air-sea transfer coefficients on bulk stability. *J. Geophys. Res. 73*, 2549–2557.

Defant, A. 1981. *The troposphere: Scientific results of the German Atlantic expedition of the research vessel "Meteor" 1925–1927.* Vol. VI, Part 1. Translation by W. J. Emery. New Delhi: Amerind Publishing Co, p. 113.

Delnore, V. E. 1972. Diurnal variation of temperature and energy budget for the oceanic mixed layer during BOMEX. *J. Phys. Oceanogr. 2*, 239–247.

Emden, E. 1913. On radiation balance and atmospheric radiation. Report of the Bavarian Academy, p. 107, Gl. 85a.

Fofonoff, N. P. 1962. Physical properties of seawater. In *The sea*, Vol. I (ed. M. N. Hill). New York: interscience, 3–20.

Friehe, C. A. and Schmitt, K. F. 1976. Parameterization of air–sea interface fluxes of sensible heat and moisture by bulk aerodynamic formulas. *J. Phys. Oceanogr. 6*, 801–809.

Halpern, D. and Reed, R. K. 1976. Heat budget of the upper ocean under light winds. *J. Phys. Oceanogr. 6*, 972–975.

Hoeber, H. 1972. Eddy thermal conductivity in the upper 12 m of the tropical Atlantic. *J. Phys. Oceanogr. 2*, 303–304.

Højerslev, N. K. 1973. Inherent and apparent optical properties of the western Mediterranean and the Hardangerfjord. *Univ. Copenhagen Inst. Phys. Oceanogr. Rep. 21*, 70 pp.

Højerslev, N. K. 1974. Inherent and apparent optical properties of the Baltic. *Univ. Copenhagen Inst. Phys. Oceanogr. Rep. 23*, 70 pp.

Howe, M. R. and Tait, R. I. 1969. Some observations of the diurnal heat wave in the ocean. *Limnol. Oceanogr. 14*, 16–22.

Husby, D. M. and Seckel, G. R. 1975. Large scale air-sea interactions at Ocean Weather Station V, 1951–1971. *NOAA Tech. Rep. NMFS, SSRF-696*, 44 pp.

Ivanoff, A. 1977. Absorption of solar energy. In *Modelling and prediction of the upper layers of the ocean* (ed. E. B. Kraus). New York: Pergamon Press, 325 pp.

Jerlov, N. G. 1951. Optical studies of ocean water. *Rep. Swedish Deep Sea Exped. 3*, 1–59.

Jerlov, N. G. 1955. Factors influencing the transparency of the Baltic waters. *Medd. Oceanogr. Inst. Göteborg 25*, 19 pp.

Jerlov, N. G. 1976. *Marine optics.* Amsterdam: Elsevier Scientific Publishing Co., 231 pp.

Kondo, J., Sasano, Y. and Ishii, T. 1979. On wind-driven currents and temperature profiles with diurnal period in the oceanic planetary boundary layer. *J. Phys. Oceanogr. 9*, 360–372.

Kullenberg, G. 1971. Vertical diffusion in shallow waters. *Tellus 23*, 129–135.

Kullenberg, G. 1974. Observed and computed scattering functions. In: *Optical aspects of oceanography* (ed. N. G. Jerlov and E. Steemann Nielsen). New York: Academic Press, 25–49.

Kullenberg, G., Lundgren, B., Malmberg, Sv.-A., Nygard, K. and Højerslev, N. K. 1970. Inherent optical properties of the Sargasso Sea. *Univ. Copenhagen Inst. Phys. Oceanogr. Rep. 11*, 18 pp.

Large, W. G. and Pond, S. 1981. Open ocean flux measurements in moderate to strong winds. *J. Phys. Oceanogr. 11*, 324–336.

Leetmaa, A. and Welch, C. S. 1972. A note on diurnal changes in momentum transfer in the surface layers of the ocean. *J. Phys. Oceanogr. 2*, 302–303.

List, R. J. 1951. *Smithsonian meteorological tables*. Washington, D.C.: Smithsonian Institution, 527 pp.

Lumb, F. E. 1964. The influence of cloud on hourly amounts of total radiation at the sea surface. *Q. J. R. Meteorol. Soc. 90*, 43–56.

Malkus, J. S. 1962. Large-scale interactions. In *The sea*, Vol. I (ed. M. H. Hill). New York: Wiley-Interscience, 88–294.

Mellor, G. L. and Durbin, P. A. 1975. The structure and dynamics of the ocean surface mixed layer. *J. Phys. Oceanogr. 5*, 718–728.

Mellor, G. L. and Yamada, T. 1974. A hierarchy of turbulence closure models for planetary boundary layers. *J. Atmos. Sci. 31*, 1791–1806.

Morel, A. 1974. Optical properties of pure water and pure sea water. In *Optical Aspects of Oceanography* (ed. N. Jerlov and E. Steemann Nielsen). New York, NY: Academic Press, 1–24.

Morel, A. and Prieur, L. 1975. Analyse spectrale des coefficients d'attenuation diffuse, de reflexion diffuse, d'absorption et de retrodiffusion pour diverses regions marines. Laboratoire d'Oceanographique Physique, Villefranche-sur-Mer, Rep. No. 17, 157 pp.

Ostapoff, F. and Worthem, S. 1974. The intra-diurnal temperature variation in the upper ocean layer. *J. Phys. Oceanogr. 4*, 601–612.

Pak, H., Beardsley, G. F. and Park, P. K. 1970. The Columbia River as a source of marine light-scattering particles. *J. Geophys. Res. 75*, 4570–4578.

Paulson, C. A. and Simpson, J. J. 1977. Irradiance measurements in the upper ocean. *J. Phys. Oceanogr. 7*, 952–956.

Payne, R. E. 1972. Albedo of the sea surface. *J. Atmos. Sci. 29*, 959–970.

Pedersen, K. and Bøyum, G. 1980. Turbulent flux of heat and water vapor from the ocean. *Tellus 32*, 320–325.

Shonting, D. H. 1964. Some observations of short-term heat transfer through the surface layers of the ocean. *Limnol. Oceanogr. 9*, 576–588.

Simpson, J. J. and Dickey, T. D. 1981a. The relationship between downward irradiance and upper ocean structure. *J. Phys. Oceanogr. 11*, 309–323.

Simpson, J. J. and Dickey, T. D. 1981b. Alternative parameterizations of downward irradiance and their dynamical significance. *J. Phys. Oceanogr. 11*, 876–882.

Simpson, J. J. and Paulson, C. A. 1979a. Observations of upper ocean temperature and salinity structure during the POLE experiment. *J. Phys. Oceanogr. 9*, 869–884.

Simpson, J. J. and Paulson, C. A. 1979b. Mid-ocean observations of atmospheric radiation. *Q. J. R. Meteorol. Soc. 105*, 487–502.

Smith, R. C. and Baker, K. S. 1981. Optical properties of the clearest natural waters (200–800 nm). *Applied Optics 20*, 177–184.

Stavn, R. H. 1982. The three-parameter model of the submarine light field: Radiant energy absorption and energy trapping in nepheloid layers. *J. Geophys. Res. 87*, 2079–2082.

Stommel, H. and Woodcock, A. H. 1951. Diurnal heating of the surface of the Gulf of Mexico in the spring of 1942. *Trans. Amer. Geophys. Un. 32*, 565–571.

Thorpe, S. A. 1977. Turbulence and mixing in a Scottish Loch. *Phil. Trans. R. Soc. London A286*, 125–181.

Trent, J. D., Shanks, A. L. and Silver, M. W. 1978. In situ and laboratory measurements on macroscopic aggregates in Monterey Bay, California. *Limnol. Oceanogr. 23*, 626–635.

Tyler, J. E. and Smith, R. C. 1970. *Measurements of spectral irradiance underwater*. New York: Gordon and Breach Science Publishers, 103 pp.

Wyrtki, K. 1966. Seasonal variations of heat exchange and surface temperature in the North Pacific Ocean. Hawaii Institute of Geophysics, *Univ. Hawaii Ref. No. HIG66-3*.

Yamada, T. 1977. A numerical experiment of pollutant dispersion in a horizontally-homogeneous atmospheric boundary layer. *Atmos. Environ. 11*, 1015–1024.

Zaneveld, J. R. V., Kitchen, J. C. and Pak, H. 1981. The influence of optical water type on the heating rate of a constant depth mixed layer. *J. Geophys. Res. 86*, 6426–6428.

Zaneveld, J. R. V., Spinrad, R. W. and Menzies, D. W. 1979. Hydrographic and optical measurements in the Congo River and Angola Basin during May 1978. School of Oceanography, Oregon State University, Corvallis, OR, Data Rep. 79–3.

Zaneveld, J. R. V. and Spinrad, R. W. 1980. An arctangent model of irradiance in the sea. *J. Geophys. Res. 85*, 4919–4922.